

RSC Advances



This is an *Accepted Manuscript*, which has been through the Royal Society of Chemistry peer review process and has been accepted for publication.

Accepted Manuscripts are published online shortly after acceptance, before technical editing, formatting and proof reading. Using this free service, authors can make their results available to the community, in citable form, before we publish the edited article. This *Accepted Manuscript* will be replaced by the edited, formatted and paginated article as soon as this is available.

You can find more information about *Accepted Manuscripts* in the [Information for Authors](#).

Please note that technical editing may introduce minor changes to the text and/or graphics, which may alter content. The journal's standard [Terms & Conditions](#) and the [Ethical guidelines](#) still apply. In no event shall the Royal Society of Chemistry be held responsible for any errors or omissions in this *Accepted Manuscript* or any consequences arising from the use of any information it contains.

1 **Direct electrochemistry of glucose oxidase immobilized on ZrO₂ nanoparticles-**
2 **decorated reduced graphene oxide sheets for a glucose biosensor**

3

4 **A.T. Ezhil Vilian^a, Shen-Ming Chen^{a*}, M. Ajmal Ali^b, Fahad M.A. Al-Hemaid^b**

5

6

7 ^aDepartment of Chemical Engineering and Biotechnology, National Taipei University of
8 Technology, No.1, Section 3, Chung-Hsiao East Road, Taipei 106, Taiwan (R.O.C).

9

10

11 ^bDepartment of Botany and Microbiology, College of Science, King Saud University,
12 Riyadh 11451, Saudi Arabia.

13

14

15

16

17

18

19

20 *Corresponding author. Fax: +886 2270 25238; Tel: +886 2270 17147,

21 E-mail: smchen78@ms15.hinet.net

22 Abstract

23 We fabricated a glucose biosensor based on glucose oxidase (GOx) immobilized in a
24 Poly (L-lysine) (PLL) and reduced graphene oxide-zirconium oxide composite (RGO-ZrO₂).
25 First, a simple single step electrochemical approach was used to prepare the RGO-ZrO₂
26 composite and its successful formation was confirmed by various techniques. Then, a mixture of
27 GOx and PLL was immobilized to form the RGO-ZrO₂ composite. Direct electrochemistry of the
28 GOx was attained for the composite film showing well-defined redox peaks centered at the
29 formal potential -0.403 V. Notably, the peak to peak separation (ΔE_p) was very low (27 mV),
30 while the heterogeneous rate constant for the fast electron transfer was calculated to be 5.03 (\pm
31 0.14 s⁻¹) revealed. The composite film modified electrode exhibited excellent electrocatalytic
32 ability through the reductive detection of oxygen. A glucose biosensor was developed using the
33 GOx-PLL/RGO-ZrO₂ composite film modified electrode which functioned using differential
34 pulse voltammetry (DPV). The fabricated biosensor exhibited good electrocatalytic ability for
35 the determination of glucose with excellent analytical parameters such as wide linear range of
36 0.29 mM to 14 mM and high sensitivity of 11.65 (\pm 0.17) $\mu\text{A mM}^{-1} \text{cm}^{-2}$. The sensor results also
37 exhibited appreciable repeatability, reproducibility and stability. Good recovery rates were
38 achieved for the real sample studies proving the promise and practicality of the proposed sensor.

39 **Keywords:** Reduced graphene oxide, zirconium oxide, glucose oxidase, electrochemistry,
40 biosensor.

41 1. Introduction

42 Graphene is a two-dimensionally arranged carbon nanomaterial that has become a rising
43 star among other carbon nanomaterials due to its exceptional electronic, mechanical and thermal
44 properties.¹⁻³ Over the past decade, graphene and graphene composites have enjoyed widespread
45 applications in numerous research areas including electronics,⁴ supercapacitors,⁵ Li-ion
46 batteries,⁶ fuel cells,⁷ sensors,⁸ and biosensors.⁹ Chemical oxidation of graphite to graphene
47 oxide (GO) and the subsequent reduction is the most popularly used approach for preparation of
48 a scalable quantity of graphene.^{8,10,11} GO, an oxygenated derivative of graphene is the important
49 starting precursor compound for the preparation of graphene-based composites.¹² Notably, GO
50 has a random arrangement of sp²/sp³ hybridized carbon atoms with plenty of oxygenated
51 functional groups, which make it highly dispersible in aqueous solutions, whereas graphene does
52 not have oxygen functionalities.¹³⁻¹⁵ Recently, numerous efforts have been made to explore the
53 preparation of graphene-based composites with metal nanoparticles,¹⁶ metal oxides,¹⁷ and
54 polymers.¹⁸ Among the aforementioned composites, the graphene-metal oxide composites have
55 drawn considerable attention for use in supercapacitors,¹⁷ solar cells,¹⁹ Li-ion batteries,²⁰ fuel
56 cells,²¹ and sensors.^{22,23} Remarkably, the graphene-metal oxide composites exhibit excellent
57 synergistic effects between the graphene and metal oxides.²²

58 ZrO₂ is an important transition metal oxide having lower toxicity and higher chemical
59 inertness, which make it more environmentally friendly.²⁴ In addition, it is highly biocompatible,
60 cheap to produce, thermally stable and electrochemically active.^{25,26} Its excellent electrocatalytic
61 properties make it a good candidate for an active electrode material for the electrocatalysis of
62 various important analytes.²⁶⁻²⁹ Electrodeposition of ZrO₂ on a self-assembled monolayer
63 template has been used for the fabrication of a modified gold electrode that can be employed for

64 the sensitive determination of parathion.³⁰ Liu *et al.* developed an electrochemical DNA
65 biosensor based on the incorporation of ZrO₂ in a boron doped diamond modified electrode.³¹
66 Specifically, ZrO₂ has been shown to have good potential for the detection of organophosphate
67 pesticides and nerve agents.²⁵ Recently, Gong *et al.* reported a simple electrochemical method
68 for the fabrication of a ZrO₂ decorated graphene hybrid for the sensing of methyl parathion.²⁶
69 Poly (L-lysine) (PLL) is a biocompatible polycationic homopolymer which is very useful in
70 promoting cell adhesion and drug delivery.^{32, 33} Positively charged PLL has been successfully
71 assembled onto a graphene surface as a linker as a consequence of the formation of the covalent
72 amide group.³⁴ PLL has drawn substantial attention in the fabrication of biosensors because of
73 its excellent ability to facilitate the transfer of electrons between the biomolecules and the
74 electrode surface.³³ Therefore, in the present work, PLL is used to immobilize glucose oxidase
75 (GOx) onto a graphene-ZrO₂ composite film modified electrode.

76 Rapid and accurate determination of the blood glucose level is very important from the
77 clinical analysis perspective to control diabetes.³⁵ Glucose oxidase (GOx) is the most widely
78 employed enzyme to make selective and sensitive glucose biosensors. The GOx enzyme, isolated
79 from *Aspergillus Niger*, consists of two identical polypeptide chains each containing
80 FAD/FADH₂ as the redox prosthetic group.^{35, 36} The key to the fabrication of efficient glucose
81 biosensors is the preparation of an appropriate matrix for the immobilization of GOx on the
82 electrode surface.³⁶ Several successful approaches have been developed over the past years for
83 the immobilization of GOx on various film modified electrodes, such as covalent attachment,³⁷
84 electrostatic interactions,³⁸ and physical adsorption.³⁹ Some of the reported glucose biosensors
85 include, electro generated magnetic nanoparticles,⁴⁰ reduced graphene oxide (RGO)-multiwalled
86 carbon nanotubes (MWCNTs),⁹ ZrO₂/Pt-PLL,⁴¹ MWCNT-Chitosan/CdSe@CdS composite

87 matrices, ⁴² sol-gel derived ZrO₂/nafion composites, ⁴³ reduced graphene oxide (RGO)/ZnO
88 composites, ⁴⁴ carbon nanotubes (CNTs)/chitosan matrices, ⁴⁴ gelatin-MWCNTs, ⁴⁵ nitrogen-
89 doped graphene, ⁴⁶ and GOx-graphene-chitosan modified electrodes. ⁴⁷

90 In the present study, we fabricate a combined RGO/ZrO₂ composite with PLL which is
91 capable of immobilizing a high amount of GOx and study its direct electrochemistry. The
92 promotion of the direct electron transfer of GOx at the RGO-ZrO₂ modified electrode and its
93 successful application for biosensing indicate that RGO-ZrO₂ could be a good candidate material
94 for the immobilization of biomolecules and the fabrication of a third-generation of biosensors.
95 The function of the fabricated GOx-PLL/RGO-ZrO₂ modified electrode as a biosensor for the
96 sensitive determination of glucose is demonstrated. The electrochemical characteristics and
97 performance of the GOx-PLL/RGO-ZrO₂ modified electrode with respect to the linear range, fast
98 response, low detection limit, high affinity, satisfactory reproducibility and accepted stability are
99 investigated in detail.

100 2. Experimental Procedure

101 2.1. Apparatus

102 The electrochemical measurements were carried out using a CHI 405 electrochemical
103 workstation. Electrochemical studies were carried out with a conventional three electrode cell
104 consisting of a modified glassy carbon electrode (GCE) as a working electrode (area 0.071 cm²),
105 Ag/AgCl (saturated KCl) as a reference electrode and PT wire as a counter electrode. Scanning
106 electron microscopic (SEM) and atomic force microscopic (AFM) characterization were carried
107 out using the S-3000H, Hitachi and CSPM4000, Being Nano-Instruments respectively. Energy-
108 dispersive X-ray (EDX) spectra studies were acquired using the HORIBA EMAX X-ACT

109 (Model 51-ADD0009, Sensor + 24V=16 W, resolution at 5.9 keV = 129 eV). The Raman spectra
110 were obtained using the Micro-Raman spectrometer (RENISHAW in the Via system, U.K) with
111 a 514.4 nm He/Ne laser. UV–visible absorption spectroscopy measurements were carried out by
112 using a Hitachi U-3300 spectrophotometer. Powder X-ray diffraction (XRD) studies were
113 performed with an XPERT-PRO (PANalytical B.V., The Netherlands) diffractometer using Cu
114 $K\alpha$ radiation ($k=1$. 54 Å). EIM6ex ZAHNER (Kroanch, Germany) was used for the
115 electrochemical impedance spectroscopy (EIS) studies. X-Ray photoelectron spectroscopy (XPS)
116 was carried out using at PHI 5000 Versa Probe equipped with an Al Kalpha X-ray source
117 (1486.6 eV).

118 2.2. Materials

119 The zirconyl chloride octahydrate ($ZrOCl_2 \cdot 8H_2O$), graphite (powder, <20 μm), poly-l-
120 lysine (PLL) and glucose oxidase (GOx, from *Aspergillus Niger*) were purchased from Sigma
121 Aldrich and used as received. All the reagents were of analytical grade and used without any
122 further purification. All the solutions were prepared using double distilled water.
123 Electrochemical studies were performed with a 0.05 M phosphate buffer solution (PBS) prepared
124 from Na_2HPO_4 and NaH_2PO_4 . A stock solution of glucose was prepared in PBS (pH 7) and the
125 solution was kept aside for one day to complete mutarotation.

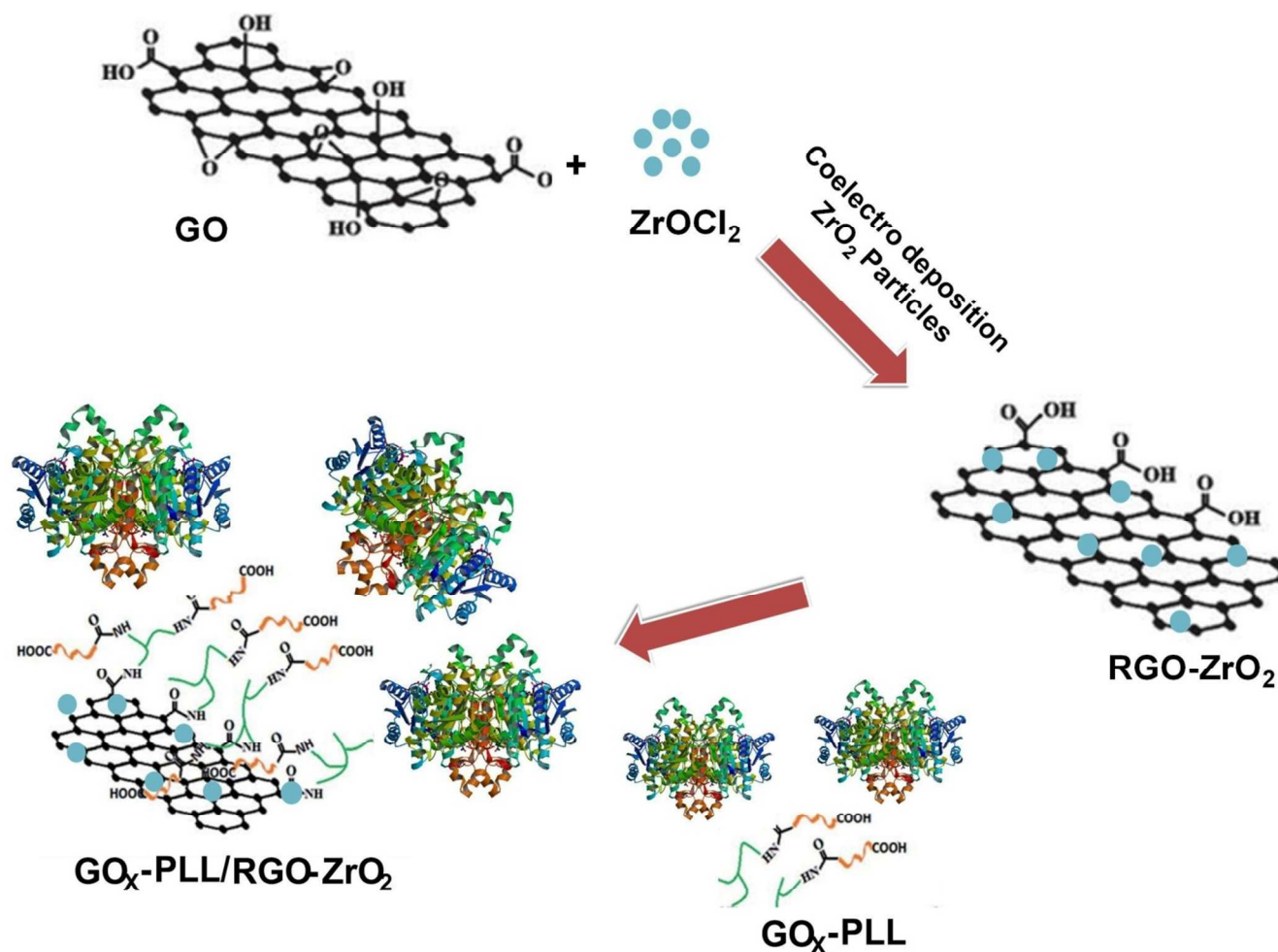
126 2.3. Electrochemical fabrication of RGO/ ZrO_2 composite modified electrode

127 Graphite oxide, synthesized from graphite using Hummer's method⁴⁸ was then dispersed
128 in water (0.5 mg/ml) and exfoliated by ultrasonication to produce graphene oxide (GO). Prior to
129 electrode modification, the GCE surface was polished with a 0.05 μm alumina slurry and
130 Buehler polishing cloth before being cleaned well with water. Afterwards, the RGO/ ZrO_2

131 composite for fabrication of the GCE was applied in a single step electrochemical process.
132 Briefly, 5 μL of the GO dispersion was drop cast onto the GCE surface and dried under ambient
133 conditions. The GO modified GCE was then moved to an electrochemical cell containing 5 mM
134 $\text{ZrOCl}_2 \cdot 8\text{H}_2\text{O}$ in PBS (pH 5). In the next step, 10 consecutive cyclic voltammograms (CVs) were
135 recorded in the potential range between 0 and -1.5 V at a scan rate 20 mV/s. The resulting
136 RGO/ ZrO_2 composite film modified GCE was rinsed with water and dried. Then 75 μL of the
137 GOx-PLL mixture (1:10) was dropped and spread out onto the surface of the RGO- ZrO_2 /GCE
138 and allowed to dry at room temperature. The modified electrode is now the GOx-PLL/RGO-
139 ZrO_2 (scheme 1). We optimized the amount of PLL and the coverage required to get the
140 maximum GOx redox peak currents. The maximum redox peak currents were observed when the
141 ratio of GOx to PLL was 1:10, so this was the ratio used in subsequent experiments.

142

143



144

145 Scheme 1. Schematic representation of the preparation procedure for the GOx-PLL/RGO-ZrO₂
 146 composite.

147

148 3. Results and discussion

149 3.1.1 SEM and EDX studies

150 The SEM image of the GO (Fig. 1A) portrays the characteristic wrinkled, crumpled and
 151 sheet like arrangement of GO sheets. The SEM image of ZrO₂ (Fig. 1B) shows a closely
 152 assembled network of ZrO₂ particles while the SEM image of RGO-ZrO₂ (Fig. 1C) presents a
 153 new morphology with a uniform distribution of numerous ZrO₂ particles on the surface of the

154 RGO sheets with a particle size ranging in a few micrometers. The morphology of the RGO-
155 ZrO₂ composite reveals a uniform decoration of numerous ZrO₂ particles over the entire region
156 of the RGO sheets. The composite has a very good porous structure which can offer a good
157 platform for the immobilization of enzymes or proteins. The SEM image of GOx-PLL/RGO-
158 ZrO₂ (Fig. 1D) shows the complete coverage of RGO-ZrO₂ by GOx-PLL. The amount of GOx
159 immobilized on the modified electrode surface (*I*) is calculated to be 1.57×10^{-10} mol cm⁻²
160 (calculated in the section 3.3). The AFM and Raman spectroscopy results also confirmed the
161 successful formation of RGO-ZrO₂ from GO and ZrO₂ (see Fig. S1 and Fig. S2).

162 **[Fig. 1]**

163 The EDX spectrum of GO (Fig. 1E) shows the presence of carbon and oxygen signals
164 with a weight percentage of 54.44 and 45.56% respectively. The oxygen signal reveals the
165 successful formation of GO from graphene. EDX spectra were obtained for the ITO glass and the
166 corresponding signal was deleted for the sake of clarification. The EDX spectrum of ZrO₂ (Fig.
167 1F) exhibited the signals for zirconium and oxygen with a weight percentage of 35.85 and
168 64.15%, respectively. The EDX spectrum of RGO-ZrO₂ (Fig. 1G) showed the signals for C, O
169 and Zr with weight percentages of 15.33, 50.72 and 32.95%, respectively. The Zr signals
170 revealed the incorporation of ZrO₂ into the RGO sheets. While the EDX spectrum for the GOx-
171 PLL/RGO-ZrO₂ exhibited the signals indicating the presence of C, O and Zr, with weight
172 percentages of 19.60, 59.59 and 20.81%, respectively (Fig. 1H).

173

174 *3.1.2 XRD and XPS studies*

175 The XRD patterns for RGO (a), ZrO₂ (b) and the RGO-ZrO₂ composite (c) are presented
176 in Fig. 2A. The XRD image of RGO shows a broad (0 0 2) diffraction peak at approximately
177 24.2°, which can be interpreted as disordered stacked graphitic sheets, indicating that the GO has
178 been reduced to RGO, while ZrO₂ exhibits its characteristic diffraction peaks at $2\theta = 30^\circ, 35^\circ,$
179 38° and 52° . Interestingly, the fact that the RGO-ZrO₂ composite exhibits all the aforementioned
180 diffraction peaks reveals the successful incorporation of ZrO₂ into RGO sheets.⁴⁹

181 [Fig. 2]

182 The XPS spectrum of the RGO-ZrO₂ composite shows the presence of the elements of
183 ZrO₂ and carbon (Fig. 2B). The peaks in the wide-scan XPS spectrum of RGO-ZrO₂ (Fig. 2B)
184 correspond to the characteristic peaks of C 1s, O 1s, and Zr 3d, indicating the existence of
185 carbon, oxygen and Zr elements in the sample. This result is consistent with the EDX elemental
186 analysis. The signal for C 1s obtained at the C=C/C-C (284.5 eV), C-O/C-O-C (hydroxyl and
187 epoxy groups, 286.4 eV), C=O (carbonyl groups, 287.8 eV), and O-C=O (carboxyl groups,
188 289.0 eV) indicates the presence of graphene sheets (see Fig. 2C), whereas signals corresponding
189 to ZrO₂, such as O 1s, were observed at 532.6. Additionally, the peaks located at 182.8 and 185.4
190 eV can be attributed to the spin-orbit splitting of the Zr 3d components, Zr 3d_{5/2}, Zr 3d_{3/2} (see
191 Fig. 2E). The binding energy of O 1s in zirconia is located at 530.1 eV. The peak positions and
192 their relative intensities are basically consistent with those for the standard cubic structure of
193 zirconia. It is noted in Fig. 2D that the peaks of Zr 3d and O 1s shift to higher binding energies
194 with increasing particle diameter. Thus, the XPS results also confirm the presence of the various
195 elements in the RGO-ZrO₂ composite⁵⁰ and are in good agreement with the XRD results.

196

197 *3.1.3 UV-visible spectroscopy and EIS studies*

198 Fig. 3A shows the UV-visible spectrum of GOx and PLL-GOx. The UV-visible spectrum
199 of GOx exhibits two well-defined absorption peaks at 380 and 455 nm which are characteristic
200 of the oxidized form of the FAD group present in GOx. The two peaks exhibited in the UV-
201 visible spectra of PLL-GOx and GOx-PLL/RGO-ZrO₂ are similar in position and shape
202 indicating that the original structural confirmation and native structure of GOx has not been
203 altered during the immobilization process.⁵¹

204

205 [Fig. 3]

206 EIS experiments were carried out in a PBS (pH 7) containing 5 mM Fe(CN)₆^{3-/4-} as the
207 supporting electrolyte at a potential of 0.5 V vs. a saturated Ag/AgCl, in the frequency range
208 between 0.1 Hz to 1 MHz. Fig. 3B shows the real and imaginary parts of the impedance spectra
209 represented as Nyquist plots (-Z_{im} vs Z_{re}) for bare GCE (a), RGO-ZrO₂ (b), GOx/RGO-ZrO₂ (c)
210 and GOx-PLL/RGO-ZrO₂ (d). The impedance values were fitted to the standard Randle's
211 equivalent circuit (see the inset to Fig. 3B) comprised of the charge transfer resistance (*Ret*),
212 ohmic resistance of the electrolyte solution (*R_s*), Warburg impedance (*Z_w*) and surface double-
213 layer capacitance (*C_{dl}*). The semicircles obtained at a lower frequency correspond to a diffusion
214 limited electron-transfer process and those obtained at a higher frequency represent a charge-
215 transfer limited process. The EIS results of the bare GCE showed a semicircular area with *Ret*
216 554Ω with decreased in diameter upon modification with RGO-ZrO₂ *Ret* 306Ω, indicating the
217 increased conductivity at the electrode surface, which can be attributed to the excellent
218 conducting properties of the RGO sheets. The EIS results for the GOx-PLL/RGO-ZrO₂ show a
219 tremendous increase in the diameter of the semicircle and a significant increase of the value of
220 *Ret* to 978Ω. The increase in the *Ret* value is indicative of increased electrical resistance at the

221 electrode surface due to the insulating bulky protein structure of the GOx. Remarkably, the
222 extent of the increase in the electrical resistance upon GOx immobilization is a measure of
223 amount of immobilization. An R_{et} of 978Ω was observed when the GOx was immobilized along
224 with PLL onto the RGO-ZrO₂, whereas an R_{et} of 703Ω was observed when the GOx was
225 immobilized without PLL. The electrical resistance was higher in the PLL incorporating
226 electrode indicating that PLL plays a significant role towards enabling high GOx loading, a
227 results which is further confirmed by the CV studies discussed in section 3.2.

228

229 3.2 Direct electrochemistry of GOx

230 The direct electrochemistry of GOx at the GOx-PLL/RGO-ZrO₂/GCE was examined by
231 cyclic voltammetry in N₂ saturated PBS (pH 7) at a scan rate of 50 mV s^{-1} (Fig. 4A). No
232 noteworthy redox peaks were observed for the RGO-ZrO₂/GCE (curve a), whereas a pair of
233 sharp well-defined redox peaks with a formal potential (E°) of -0.416 V (FAD/FADH₂) were
234 observed for the GOx-PLL/RGO-ZrO₂ (curve c). These revealed the direct electron transfer of
235 GOx. The greatly enhanced peak currents and very low peak to peak separation (ΔE_p) 27 mV
236 show the fast and efficient electrical communication between the modified electrode surface and
237 the active GOx sites. The large surface area and high conductivity of the composite are the
238 probable reasons for the greatly enhanced direct electrochemical behavior of the GOx. In order
239 to understand the role of PLL, we carried out cyclic voltammetry without the addition of PLL
240 into the electrode matrix. The feeble redox pairs of GOx with E° -0.417 V and ΔE_p 125 mV
241 observed at the GOx/RGO-ZrO₂/GCE (curve b) show the lack of efficient electrical
242 communication of the modified electrode with the GOx. On the other hand, the direct electron
243 transfer of GOx was greatly enhanced after the inclusion of PLL into the electrode matrix. This

244 result shows the crucial role of PLL towards promoting electrical communication between the
245 modified electrode surface and the GOx. The stability of the GOx-PLL/RGO-ZrO₂ in PBS (pH 7)
246 was also studied by scanning 500 continuous potentials at a scan rate of 50 mVs⁻¹. It was found
247 that 94.42% of the initial peak current was retained even after 500 continuous cycles, revealing
248 the outstanding stability of the modified film (Fig. S3A). On the other hand, for the GOx/RGO-
249 ZrO₂/GCE, only about 79.87% of the initial peak current was retained after 500 continuous
250 cycles (Fig. S3B), showing the poor stability of the electrode without PLL. We also investigated
251 the individual role of RGO and ZrO₂ towards the direct electrochemistry of the GOx and glucose
252 sensors and assessed their special roles (Fig. S4). On the whole, GOx-PLL/RGO-ZrO₂ has been
253 proved to be an excellent matrix for the direct electrochemistry of GOx, creating a good
254 biocompatible environment for maintaining the bioactivity of the enzyme.

255 **[Fig. 4]**

256 3.3 Effect of scan rate and different pHs

257 The effect of the scan rate on the redox behavior of GOx in PBS (pH 7) was examined.
258 There was a linear increase in both I_{pa} and I_{pc} as the scan rate increased from 0.1 to 1 V s⁻¹ (Fig.
259 4B). A plot of the peak current versus the scan rate reveals a linear relationship which shows that
260 the direct electron transfer of GOx is a surface-controlled process (inset to Fig. 4B). The linear
261 regression equations for the anodic and cathodic process can be expressed as $I_{pa}/\mu A = 40.83$
262 $(\pm 0.38)v/(\mu A/Vs^{-1}) + 4.54(\pm 0.13)/\mu A$, $R^2=0.996$ and $I_{pc}/\mu A = -38.85(\pm 0.25)v/(\mu A/Vs^{-1}) - 4.016$
263 $(\pm 0.14)/\mu A$, $R^2=0.995$, respectively.

264 The heterogeneous electron transfer rate constant (k_s) between GOx and the modified
265 electrode was calculated using the Laviron eq. (1)⁹. ($n\Delta E_p > 0.200$ V),

266

267
$$\text{Log}(k_s/s^{-1}) = \alpha \log(1 - \alpha) + (1 - \alpha) \log \alpha - \log[(RT/nFv)(1/s)] - \alpha(1 - \alpha)nF\Delta E_p/2.3RT \quad (1)$$

268

269 where α is the charge transfer coefficient (calculated to be 0.5 using the Tafel equation),⁵² v is
270 the scan rate in V s^{-1} , n is the number of electrons, and the other parameters R , T and F represent
271 their usual meanings. The k_s value at the GOx-PLL/RGO-ZrO₂ is calculated to be 5.03 s^{-1} , which
272 is comparatively larger than the values reported in the literature, for instance for the MWNT-
273 Chitosan/CdSe@CdS composite (1.56 s^{-1})⁴², glucose oxidase-graphene-chitosan (2.83 s^{-1}),⁴⁷ or
274 MWNT-coated electrospun gold fibers (1.12 s^{-1}).⁵³ The comparatively higher k_s value achieved
275 for the GOx-PLL/RGO-ZrO₂ is indicative of the occurrence of rapid electron transfer between
276 the active redox sites for GOx at the modified electrode surface. The amount of electroactive
277 GOx available on the electrode surface (Γ) was calculated to be $1.568 \times 10^{-10} \text{ mol cm}^{-2}$, which is
278 higher than the theoretical monolayer coverage of GOx.⁴⁵

279 The redox coupling of GOx at the GOx-PLL/RGO-ZrO₂ is confirmed by the stable well-
280 defined and voltammetric redox peaks exhibited over the entire pH range from 1 to 9 (Fig. S6A).
281 The pH and $E^{\circ'}$ (Fig. S6B) are plotted and show a linear relationship. The respective linear
282 regression equation can be expressed as $E^{\circ'}/\text{V} = -0.0414 (\pm 0.51) / \text{V} - 0.0578 (\pm 0.40) \text{ pH}/$
283 (V/pH) , $R^2 = 0.998$. Here the slope value is $-57.8 \text{ V}/\text{pH}$, which is close to the theoretical value
284 obtained with the Nernst equation ($-58.6 \text{ mV}/\text{pH}$) for the transfer process for an equal number of
285 protons and electrons. Thus, the electron transfer process of the FAD/FADH₂ redox couples
286 reported in this study involves an equal number of protons and electrons which is consistent with
287 the results reported in the literature.^{9, 45}

288 3.4 Determination of glucose

289 Fig. 5 shows CVs for GOx-PLL/RGO-ZrO₂ in an oxygen saturated PBS (pH 7) for
290 various glucose concentrations obtained after additions of 1 mM (b to e). A sharp voltammetric
291 peak is observed in the presence of glucose at a potential of -0.45 V which is responsible for the
292 electrochemical reduction of oxygen. The reactions occurring at the electrode surface can be
293 explained as follows:

294



298

299 The glucose was oxidized by the GOx to form gluconolactone, while the oxidized form
300 of GOx (FAD) was converted to the reduced form of GOx (FADH₂) (eq. 2). Subsequently, the
301 FADH₂ was reoxidised to form FAD by consuming oxygen (eq. 3). Finally the reductive
302 detection of oxygen consumption was monitored at a potential of -0.45 V (eq. 4). There was a
303 decrease in the peak reduction current responsible for the reduction of oxygen upon addition of
304 the glucose. The linear decrease in the reduction peak current with the consumption of oxygen
305 revealed the efficient electrocatalytic reduction of oxygen at the GOx-PLL/RGO-ZrO₂/GCE. As
306 expected, the GOx-PLL/RGO-ZrO₂/GCE exhibited better electrocatalytic activity for glucose
307 biosensing than the GOx-PLL/ZrO₂/GCE or GOx-PLL/RGO modified GCE (See Fig.S5A and
308 B). It is known that very high over-potentials are required for the electrocatalytic activity of
309 glucose at the GOx-PLL/ZrO₂/GCE and thus no obvious redox peaks were observed in this
310 electrochemical window (See Fig.S5B). In comparison with those for the GOx-PLL/ZrO₂/GCE
311 and GOx-PLL/RGO modified GCE, a remarkable decrease in reduction current and positive shift

312 of the peak potential can be observed for the GOx-PLL/RGO modified GCE, however it
313 demonstrated less electrocatalytic activity than that of the GOx-PLL/RGO-ZrO₂/GCE. All these
314 observations indicate the excellent electrocatalytic capability of the GOx-PLL/RGO-ZrO₂/GCE
315 for glucose biosensing (See Fig. 5). We speculate that it was the high surface area of the RGO-
316 ZrO₂ films that increased the capacity for GOx-PLL immobilization, facilitating faster electron-
317 transfer kinetics for glucose biosensing and electrocatalytic activity.

318 **[Fig. 5]**

319 Further, we also investigated the contribution of PLL towards glucose biosensing. Fig. S7
320 (A) shows the CVs obtained at the GOx/RGO-ZrO₂/GCE (A) in the absence (a) and presence of
321 3 mM glucose (b) in PBS (pH 7) at a scan rate 50 mV s⁻¹. In the absence of glucose there was a
322 sharp reduction peak observed at the potential of -0.45 V which can be attributed to the oxygen
323 reduction. No obvious increase in the peak current was observed upon the addition of glucose,
324 indicating that the modified electrode did not have the electrocatalytic ability to sense glucose.
325 Fig. S7 (B) shows the CVs obtained at the GOx-PLL/RGO-ZrO₂ (A) in the absence (a) and
326 presence of 3 mM glucose (b) in PBS (pH 7). A sharp increase in the peak current was observed
327 upon addition of 3 mM of glucose indicating the excellent electrocatalytic ability of the PLL
328 containing modified electrode for glucose biosensing. Thus PLL plays a major role in the GOx-
329 PLL/RGO-ZrO₂ composite towards the determination of glucose.

330

331 *3.5 Biosensing of glucose at GOx-PLL/RGO-ZrO₂/GCE*

332 Fig. 6A shows the DPVs for the GOx-PLL/RGO-ZrO₂ in an oxygen saturated PBS (pH
333 7) with various concentrations of glucose. In the absence of glucose, a sharp peak was observed

334 at the potential -0.4 V which can be ascribed to the reduction of oxygen. There was a decrease in
335 the peak current after the addition of 0.29 mM glucose. The peak current decreased linearly upon
336 further addition of glucose indicating the consumption of oxygen after each addition. This could
337 be attributed to the good electrocatalytic ability of the GOx-PLL/RGO-ZrO₂ modified electrode
338 for the efficient reduction of oxygen, which would indirectly assist in the monitoring of the
339 concentration of glucose.

340 **[Fig. 6]**

341 A linear calibration plot was made between the concentration of glucose and the peak
342 current (Fig. 6B). The linear regression equation can be expressed as $I_p(\mu\text{A}) = 2.797 (\pm 0.041) +$
343 $100.6 (\pm 0.072) C_{\text{glucose}} (\text{mM}), R^2 = 0.992$. The fabricated biosensor exhibited a wide linear range
344 between 0.29 and 14 mM. The sensitivity of the biosensor calculated from the slope of the
345 calibration plot was determined to be $11.65 (\pm 0.17) \mu\text{A mM}^{-1} \text{cm}^{-2}$. The limit of detection (LOD)
346 was calculated to be $0.13 (\pm 0.021) \text{mM}$. Here, the LOD was calculated using the formula, $\text{LOD} =$
347 $3 s_b/S$, where s_b is the standard deviation of ten blank measurements and S is the sensitivity.⁵⁴
348 The important analytical parameters were compared with those for reported for other sensors
349 available in past studies (Table 1). As can be seen from Table 1, the GOx-PLL/RGO-ZrO₂
350 offered a quite comparable analytical performance. The results revealed the good capability of
351 the sensor towards the determination of glucose. The DPV technique, which is very sensitive,
352 selective and does not require hydrodynamic conditions as in the case amperometric technique,
353 was used.

354 **[Table 1]**

355 3.6 Determination of glucose in urine samples

356 The practicality of the proposed sensor was also investigated by testing urine samples
357 collected from a diabetes patient. The amount of glucose present in the urine sample was pre-
358 determined by photometric analysis with a ROCHE COBAS C 111 ANALYZER to be 6.423
359 mM. Then the amount of glucose was also determined using the GOx-PLL/RGO-ZrO₂ modified
360 electrode via DPV. The standard addition method was adopted to calculate the concentration of
361 glucose and it was found to be 6.744 mM, a result which is in good agreement with the
362 photometric analysis. This confirms that the proposed sensor can be useful for the determination
363 of glucose present in human urine samples.

364 Next, urine samples collected from a healthy man were diluted in 0.1 M PBS at a
365 ratio of 1: 100. Known concentrations of glucose samples were spiked into the urine samples
366 which were analyzed using the GOx-PLL/RGO-ZrO₂/GCE (Fig. S8). Fig. S8 presents the CVs
367 obtained for the GOx-PLL/RGO-ZrO₂/GCE for urine samples without (a) with 1 mM (b), 2 mM
368 (c), 3 mM (d) and 4 mM glucose (e); the scan rate was 50 mV s⁻¹. Recovery rates were
369 calculated from the CV results. Comparison of the values for the spiked samples and determined
370 samples exhibited good recoveries from 97 to 102.5%, as shown in table 2. Good recoveries
371 achieved for the determination of glucose in the spiked human urine samples revealed the
372 practicality of the proposed biosensor.

373 *3.7 Stability, repeatability and reproducibility studies*

374 The repeatability of using the same GOx-PLL/RGO-ZrO₂ modified electrode was
375 examined. In the tests we used 1 mM of glucose in a 0.1 M pH 7.0 PBS. Results showed that the
376 relative standard deviation for 5 determinations was 2.57 % (see Fig. S9). In addition, the
377 relative standard deviation of the current signals for measurement of 1 mM glucose in 0.1 M pH
378 7.0 PBS for 6 independently prepared biosensors was determined to be 2.6 %, which proves the

379 good reproducibility of the biosensor preparation process (see Fig. S10). On the other hand, the
380 long-term stability of the proposed biosensor was also estimated by measuring its response to a 1
381 mM glucose solution after the electrode had been stored in a dry state at 4 °C for 1 month. The
382 biosensor retained 94.4% of its original response after 1 month, which proves that the RGO-ZrO₂
383 efficiently maintained the activity of GOx (see Fig. S11). The appreciable stability, repeatability
384 and reproducibility results achieved indicate that the GOx-PLL/RGO-ZrO₂ modified electrode
385 based sensor is a versatile sensor for the determination of glucose.

386 **4. Conclusion**

387 A GOx-PLL/RGO-ZrO₂ modified electrode was prepared by a simple electrochemical
388 process. The direct electrochemistry of the GOx showed greatly enhanced redox peak currents
389 and fast electron transfer constants. The modified electrode exhibited excellent electrocatalytic
390 ability towards the determination of glucose by the reductive detection of oxygen. The developed
391 biosensor exhibited good analytical parameters for efficient glucose determination by the DPV
392 technique. In addition, the sensor offered good repeatability, reproducibility and stability results.
393 The excellent performances of the prepared composite film can also be explored for the
394 immobilization of other redox enzymes or proteins.

395 **Acknowledgement**

396 This Research was supported by the King Saud University, Deanship of Scientific
397 Research, College of Science, Research Center.

398 **References**

- 399 1. V. Singh, D. Joung, L. Zhai, S. Das, S.I. Khondaker, S. Seal, *Prog. Mater. Sci.* 2011, **56**
400 1178-1271.
- 401 2. A.K. Geim, *Science*, 2009, **324**, 1530-1534.
- 402 3. Y. Dong, H. Pang, H.B. Yang, C. Guo, J. Shao, Y. Chi, C.M. Li, T. Yu, *Angew. Chem.*
403 *Int. Ed.* 2013, **30**, 7800-7804.
- 404 4. X. Wu, M. Sprinkle, X. Li, F. Ming, C. Berger, W.A.D Heer, *Phys. Rev. Lett.* 2008, **101**,
405 026801.
- 406 5. J.J. Yoo, K. Balakrishnan, J. Huang, V. Meunier, B.G. Sumpter, Srivastava, M. Conway,
407 A.L.M. Reddy, J. Yu, R. Vajtai, P.M. Ajayan, *Nano Lett.* 2011, **11**, 1423-1427.
- 408 6. S. Yang, G. Cui, S. Pang, Q. Cao, U. Kolb, X. Feng, J. Maier, K. Mullen, *Chem Sus*
409 *Chem*, 2010, **3**, 236-239.
- 410 7. C.X. Guo, L.Y. Zhang, J. Miao, J. Zhang, C.M. Li, *Adv. Energy Mater.* 2013**3**, 167-171.
- 411 8. V. Mani, A.P. Periasamy, S.M. Chen, *Electrochem. Commun.* 2012, **17**,75-78
- 412 9. V. Mani, B. Devadas, S.M. Chen, *Biosens. Bioelectron.* 2013, **41**, 309-315.
- 413 10. M. Pumera, A. Ambrosi, A. Bonanni, E.L.K. Chng, H.L. Poh, *TrAC, Trends Anal.*
414 *Chem.* 2010, **29**, 954-965.
- 415 11. S. Park, J. An, J.R. Potts, A. Velamakanni, S. Murali, R.S. Ruoff, *Carbon*, 2011, **49**,
416 3019-3023.
- 417 12. D. Chen, H. Feng, J. Li, *Chem. Rev.* 2012, **112**, 6027-6053.
- 418 13. S. Kim, S. Zhou, Y. Hu, M. Acik, Y.J. Chabal, C. Berger, W. Heer, A. Bongiorno, E.
419 Riedo, *Nat. mater.* 2012, **11**, 544-549.
- 420 14. S. Stankovich, R. Piner, S.T. Nguyen, R.S. Ruoff, *Carbon*, 2006, **44**, 3342-3347.

- 421 15. Z.B. Liu, Y.F. Xu, X.Y. Zhang, X.L. Zhang, Y.S. Chen, J.G. Tian, *J. Phys. Chem. B*,
422 2009, **113**, 9681-9686.
- 423 16. Q. Zhuo, Y. Ma, J. Gao, P. Zhang, Y. Xia, Y. Tian, X. Sun, J. Zhong, X. Sun, *Inorg.*
424 *Chem.*2013, **52**, 3141-3147.
- 425 17. S. Chen, J. Zhu, X. Wu, Q. Han, X. Wang, *ACS nano*, 2010, **4**, 2822-2830.
- 426 18. Y. Sun, G. Shi, *J. Polym. Sci., Part B: Polym. Phys.*2013, **51**, 231-253.
- 427 19. S. Sun, L. Gao, Y. Liu, *Appl. Phys. Lett.*, 2010, **96**, 083113(1-3).
- 428 20. G. Wang, J. Liu, S. Tang, H. Li, D. Cao, *J. Solid State Electrochem.*2011, **15**, 2587-
429 2592.
- 430 21. Y. Liang, Y. Li, H. Wang, J. Zhou, J. Wang, T. Regier, H. Dai, *Nat. mater.*,2011,
431 **10**,780-786.
- 432 22. G. Singh, A. Choudhary, D. Haranath, A.G. Joshi, N. Singh, S. Singh, R. Pasricha,
433 *Carbon*, 2012, **50**, 385-394.
- 434 23. L. Peng, X. Peng, B. Liu, C. Wu, Y. Xie, G. Yu, *Nano Lett.*, 2013, **13**, 2151-2157.
- 435 24. B. Liu, J. Hu, J.S. Foord, *Electrochem.Solid-State Lett.*, 2011, **14**, D20-D22.
- 436 25. G. Liu, Y. Lin, *Anal. Chem.*2005, **77**, 5894-5901.
- 437 26. J. Gong, X. Miao, H. Wan, D. Song, *Sens. Actuators, B* 2012, **162**, 341-347.
- 438 27. W. Sun, X. Wang, Xi. Sun, Y. Deng, J. Liu, B. Lei, Z. Sun, *Biosens. Bioelectron.* 2013,
439 **44**, 146-151.
- 440 28. M. Das, C. Dhand, G. Sumana, A.K. Srivastava, R. Nagarajan, L. Nain, M. Iwamoto, T.
441 Manaka, B.D. Malhotra, *Biomacromolecules*,2011,**12**,540-547.
- 442 29. Z. Tong, R. Yuan, Y. Chai, S. Chen, Y. Xie, *Biotechnol. Lett.* 2007, **29**, 791-795.
- 443 30. J.H. Zhou, C.Y. Deng, S.H. Si, S.E. Wang, *Microchim. Acta*, 2011, **172**, 207-215.

- 444 31. B. Liu, J. Hu, J.S. Foord, *Electrochem. Commun.* 2012, **19**, 46-49.
- 445 32. S. Some, S.M. Ho, P. Dua, E. Hwang, Y.H. Shin, H.J. Yoo, J.S. Kang, D.K. Lee, H. Lee,
446 *ACS Nano* 2012, **6**, 7151-7161.
- 447 33. C. Shan, H. Yang, D. Han, Q. Zhang, A. Ivaska, L. Niu, *Langmuir*,2009,**25**,12030-
448 12033.
- 449 34. D. Zhang, Y. Zhang, L. Zheng, Y. Zhan, L. He, *Biosens. Bioelectron.*2013, **42**, 112-118.
- 450 35. C.X. Guo, C.M. Li, *Phys. Chem. Chem. Phys.* 2010, **12**, 12153-12159.
- 451 36. Z. Luo, L. Yuwen, Y. Han, J. Tian, X. Zhu, L. Weng, L. Wang, *Biosens. Bioelectron.*
452 2012, **36**, 179-185.
- 453 37. S. Zhang, N. Wang, H. Yu, Y. Niu, C. Sun, *Bioelectrochemistry*, 2005, **67**, 15-22.
- 454 38. Z. Ma, T. Ding, *Nanoscale Res. Lett.* 2009, **4**, 1236-1240.
- 455 39. W.Z. Jia, K. Wang, Z.J. Zhu, H.T. Song, X.H. Xia, *Langmuir*, 2007, **23**, 11896-11900.
- 456 40. F.N. Comba, M.D. Rubianes, L. Cabrera, S. Gutierrez, P. Herrasti, G.A. Rivasa,
457 *Electroanalysis*,2010,**22**, 1566-1572.
- 458 41. X. Yang, Q. Zhang, Y. Sun, S. Liu, *IEEE sens. J.* 2007, **7**, 1735-1741.
- 459 42. F. Huang, F. Wang, S. Feng, Y. Li, S. Li, Y. Li, *J. Solid State Electrochem.*2013,**17**,
460 1295-1301.
- 461 43. H.J. Kim, S.H. Yoon, H.N. Choi, Y.K. Lyu, W.Y. Lee, *Bull. Korean Chem. Soc.* 2006,
462 **27**, 65-70.
- 463 44. Y. Liu, M. Wang, F. Zhao, Z. Xu, S. Dong, *Biosens. Bioelectron.* 2005, **21**, 984-988.
- 464 45. A.P. Periasamy, Y.J. Chang, S.M. Chen, *Bioelectrochemistry*, 2011, **80**, 14-120.
- 465 46. Y. Wang, Y. Shao, D. W. Matson, J. Li, Y. Lin, *ACS nano*, 2010, 4,1790-1798.

- 466 47. X. Kang, J. Wang, H. Wu, I.A. Aksay, J. Liu, Y. Lin, *Biosens. Bioelectron.* 2009, **25**,
467 901-905.
- 468 48. W.S. Hummers, R.E. Offeman, *J. Am. Chem. Soc.* 1958, **80**, 1339.
- 469 49. C.J. Cai, M.W. Xu, S.J. Bao, C. Lei, D.Z. Jia, *RSC Adv.* 2012, **2**, 8172-8178.
- 470 50. M. Niasari, M. Dadkhah, F. Davar, *Polyhedron*, 2009, **28**, 3 005-3009.
- 471 51. H. Liu, N. Hu, *Electroanalysis*, 2007, **19**, 884-892.
- 472 52. A.J. Bard, L.R. Faulkner, *2nd Ed. Wiley, New York.* 2001.
- 473 53. M.V. Jose, S. Marx, H. Murata, R.R. Koepsel, A.J. Russell, *Carbon* 2012, **50**, 4010-
474 4020.
- 475 54. A. Radoi, D. Compagnone, E. Devic, G. Palleschi, *Sens. Actuators, B* 2007, **121**, 501-
476 506.
- 477 55. X. Xiao, B. Zhou, L. Zhu, L. Xu, L. Tan, H. Tang, Y. Zhang, Q. Xie, S. Yao, *Sens.*
478 *Actuators, B* 2012, **165**, 126-132.
- 479 56. W. Zhao, Y. Ni, Q. Zhu, R. Fu, X. Huang, J. Shen, *Biosens. Bioelectron.* 2013, **44**, 1-5.
- 480 57. S. Liu, H. Ju, *Biosens. Bioelectron.* 2003, **19**, 177-183.
- 481 58. Y.L. Yao, K.K. Shiu, *Electroanalysis*, 2008, **20**, 1542-1548.
- 482 59. B. Haghighi, M.A. Tabrizi, *Colloids Surf., B* 2013, **103**, 566-571.
- 483 60. Z.J. Yang, Y.Y. Ren, Y.C. Zhang, J. Li, H.B. Li, X.C. Huang, X.Y. Hu, Q. Xu, *Biosens.*
484 *Bioelectron.* 2011, **26**, 4337-4341.
- 485 61. S. Tang, X.Z. Wang, J.P. Lei, Z. Hu, S.Y. Deng, H.X. Ju, *Biosens. Bioelectron.* 2010, **26**,
486 432-436.
- 487 62. Y.L. Wang, L. Liu, M.G. Li, S.D. Xu, F. Gao, *Biosens. Bioelectron.* 2011, **30**, 107-111.
- 488 63. S. Palanisamy, C. Karupiah, S. Chen, *Colloids Surf., B*, 2014, 114, 164-169.

489 **Table 1**

490 Comparison of the electroanalytical parameters of the GOx-PLL/RGO-ZrO₂ with other GOx-
 491 based modified electrodes

Electrode	Method	Linear range/mM	Sensitivity μA/mM/cm ²	Ref.
GOx- ^a PMB@SiO _{2(nano)}	DPV	0.01-1.11	-	55
GOx/(SiO ₂ - ^b PA)	DPV	0.016 -8	-	56
GOx/colloidal Au	CV	0.04 - 0.28	8.4	57
^c PDDA-GOx/Au/CNT	Amperometry	0.5-5.0	2.5	58
^d OOPPy-nanoAu/GOx	Amperometry	1- 8	-	59
GOx/SnS ₂ /Nafion/GCE	Amperometry	0.025-1.1	7.6	60
GOx/Pt ^e FCNA/GCE	Amperometry	0.5-8.0	6.0	61
Nafion/GOx/Ag/ ^f Pdop@CNT/GCE	Amperometry	0.05-1.1	3.1	62
RGO/Ag/GOx	CV	0.5-12.5	3.84	63
GOx-PLL/RGO-ZrO ₂	DPV	0.29 -14	11.65 (± 0.17)	Our work

492

493 ^a poly(methylene blue) ^b phytic acid ^c Poly(diallyldimethylammonium chloride) ^d overoxidized
 494 polypyrrole ^eflower-like carbon nanosheet aggregation. ^fpolydopamine.

495

496

497 **Figure Captions**

498

499 **Fig. 1** SEM images of GO (A), ZrO₂ (B), RGO-ZrO₂ (C) and GOx-PLL/RGO-ZrO₂ (D). EDX
500 images of GO (E), ZrO₂ (F), RGO-ZrO₂ (G) and GOx-PLL/RGO-ZrO₂ (H).

501

502 **Fig. 2** (A) XRD patterns of RGO (a), ZrO₂ (b) and RGO-ZrO₂ composite (c). (B) XPS spectrum
503 of RGO-ZrO₂ composite, (C) C 1s XPS spectra of RGO-ZrO₂ composite, (D) deconvoluted O 1s
504 spectra of RGO-ZrO₂ composite, (E) Zr 3d core-level spectrum of the RGO-ZrO₂ composite,

505

506 **Fig. 3** (A) UV-Vis spectra of GOx, GOx-PLL and GOx-PLL/RGO-ZrO₂. (B) Nyquist plots from
507 EIS results for bare GCE (a), ZrO₂/GCE (b), RGO-ZrO₂/GCE (c), GOx-PLL/RGO-ZrO₂ (d) in
508 PBS (pH 7) containing 5 mM Fe(CN)₆^{3-/4-}. Inset: Randles equivalent circuit model.

509

510 **Fig. 4** (A) CVs of bare (a) RGO-ZrO₂ (b) and GOx-PLL/RGO-ZrO₂ (c) film modified GCEs in
511 0.05 M nitrogen-saturated PBS (pH 7) at the scan rate 50 mV s⁻¹. (B) CVs of GOx-PLL/RGO-
512 ZrO₂ in PBS (pH 7) at the different scan rates from 0.1 to 1 V s⁻¹. Inset: Plot of I_{pa} and I_{pc} versus
513 scan rates. $I_p/\mu\text{A}$ is presented as a function of $v/(\text{Vs}^{-1})$, $I_{pa}/\mu\text{A} = 40.83 (\pm 0.38) v/(\mu\text{A}/\text{Vs}^{-1}) +$
514 $4.54(\pm 0.13)/\mu\text{A}$, $R^2=0.996$ and $I_{pc}/\mu\text{A} = -38.85 (\pm 0.25) v/(\mu\text{A}/\text{Vs}^{-1}) - 4.016 (\pm 0.14) /\mu\text{A}$,
515 $R^2=0.995$ respectively. Error bars represent the standard deviation for 3 independent
516 measurements.

517

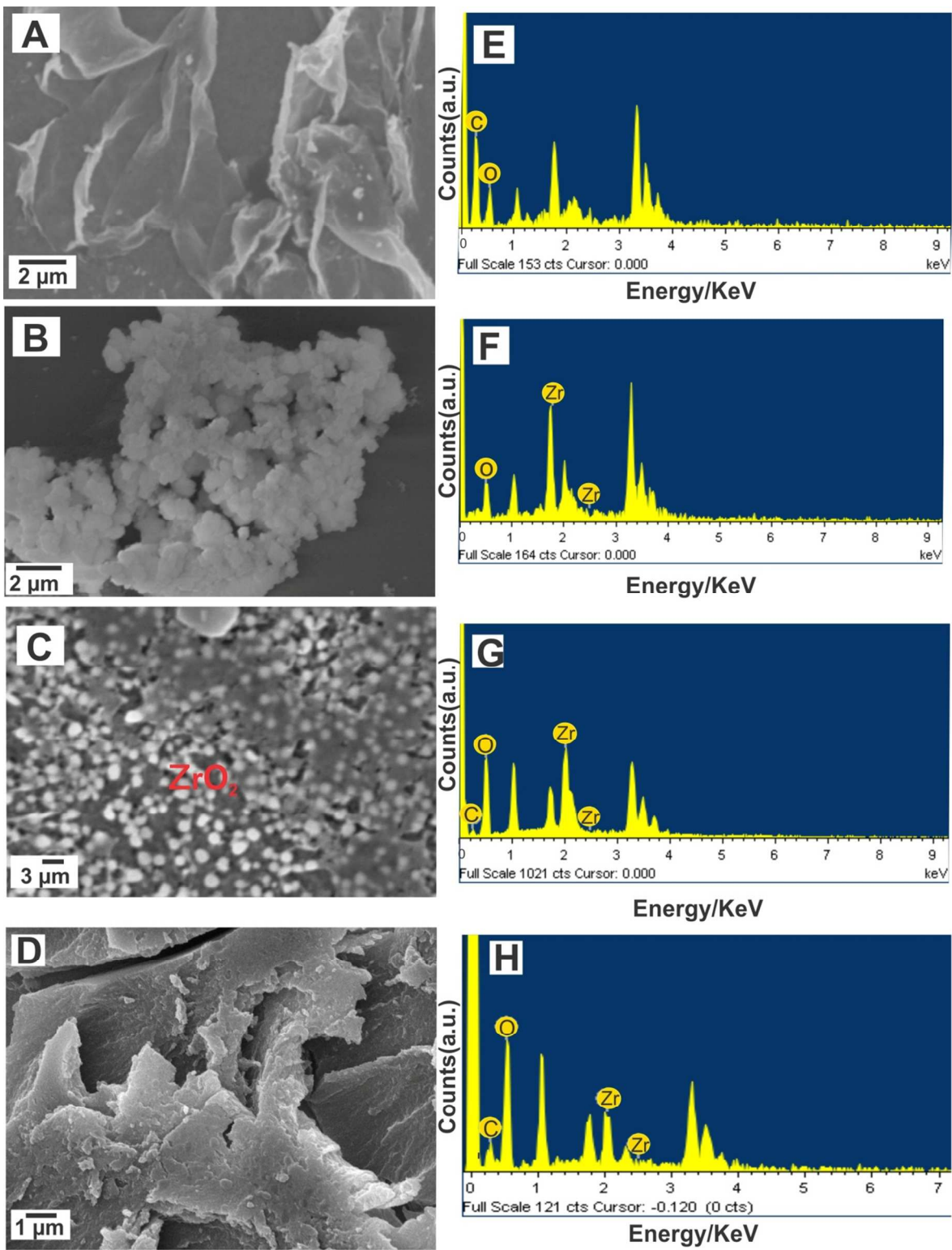
518 **Fig. 5** CVs of GOx-PLL/RGO-ZrO₂ in oxygen saturated PBS (pH 7) containing various
519 concentrations of glucose 0 (a), 1 (b), 1.96 (c), 2.91 (d) and 3.84 mM (e) at a scan rate 50 mV s⁻¹.

520

521 **Fig. 6** (A) DPVs of GOx-PLL/RGO-ZrO₂ in oxygen saturated PBS (pH 7) without glucose (a)
522 and with glucose concentrations ranging from 1 to 7 mM (b to h). (B) Plot of response current vs.
523 concentration of glucose. $I_p(\mu\text{A}) = 2.797 (\pm 0.041) + 100.6 (\pm 0.072) C_{\text{glucose}} (\text{mM})$, $R^2 = 0.992$.
524 Error bars represent the standard deviation of 3 independent experiments.

525

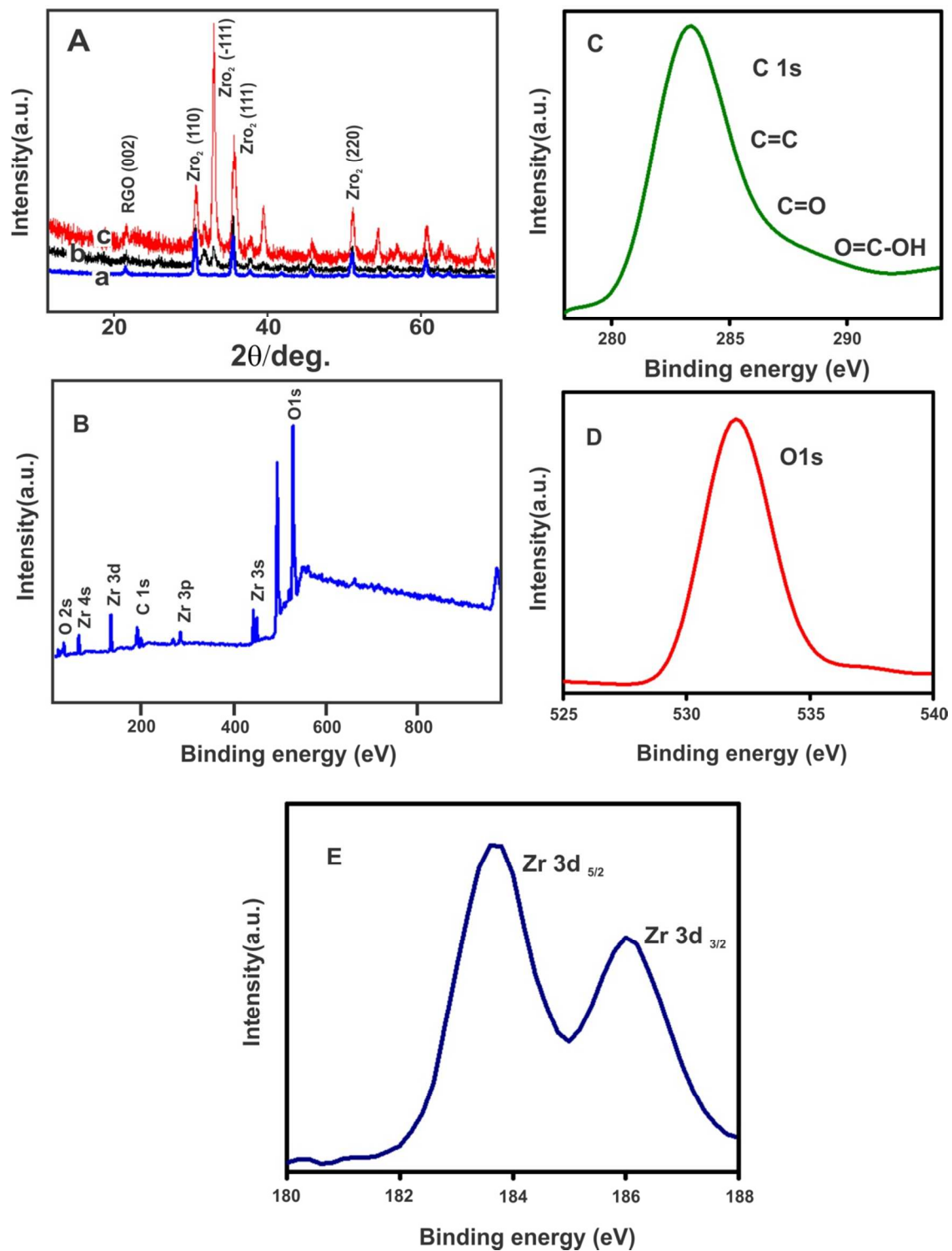
Figures



526

527

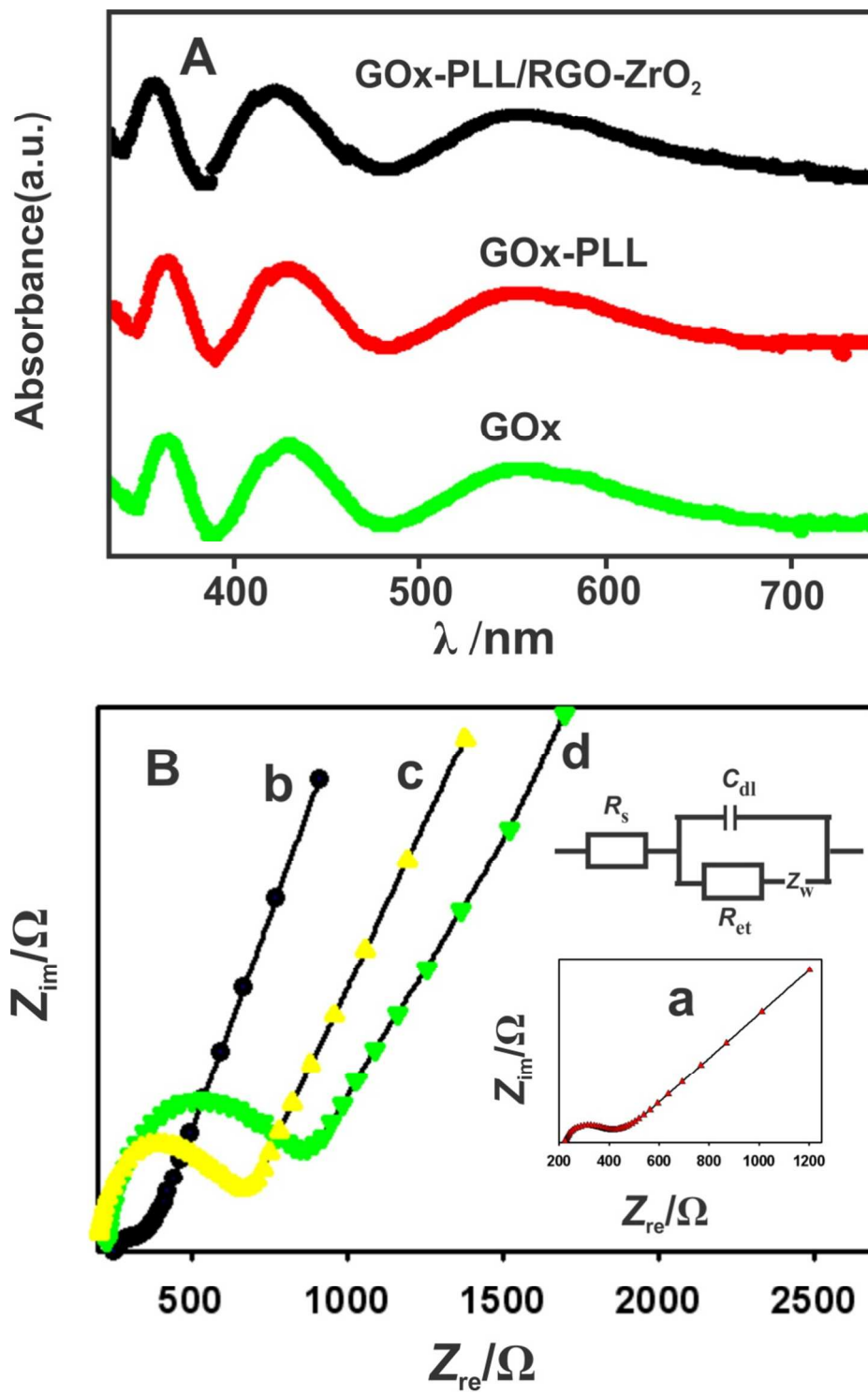
Fig. 1.



528

529

Fig. 2

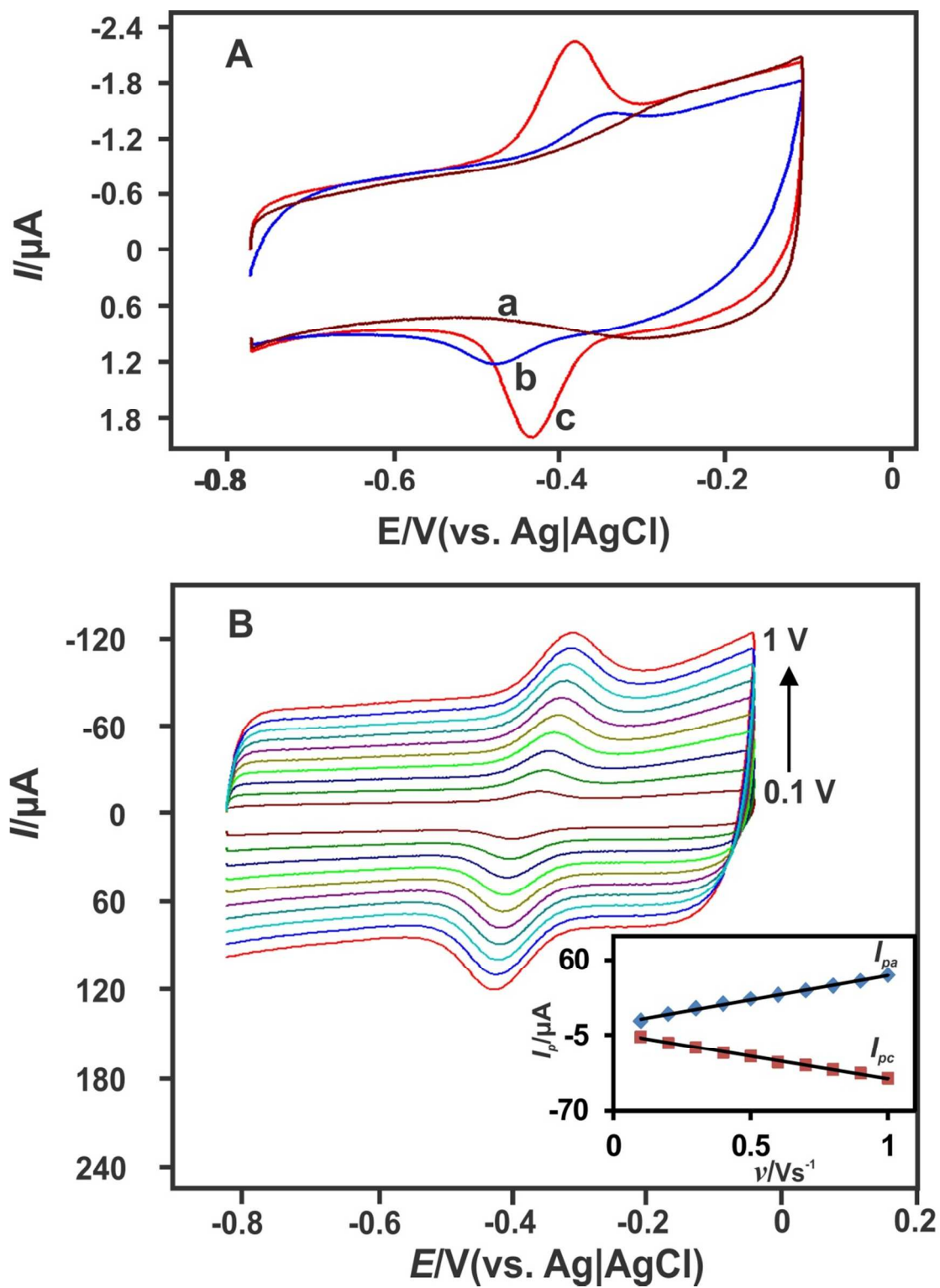


530

531

532

Fig. 3

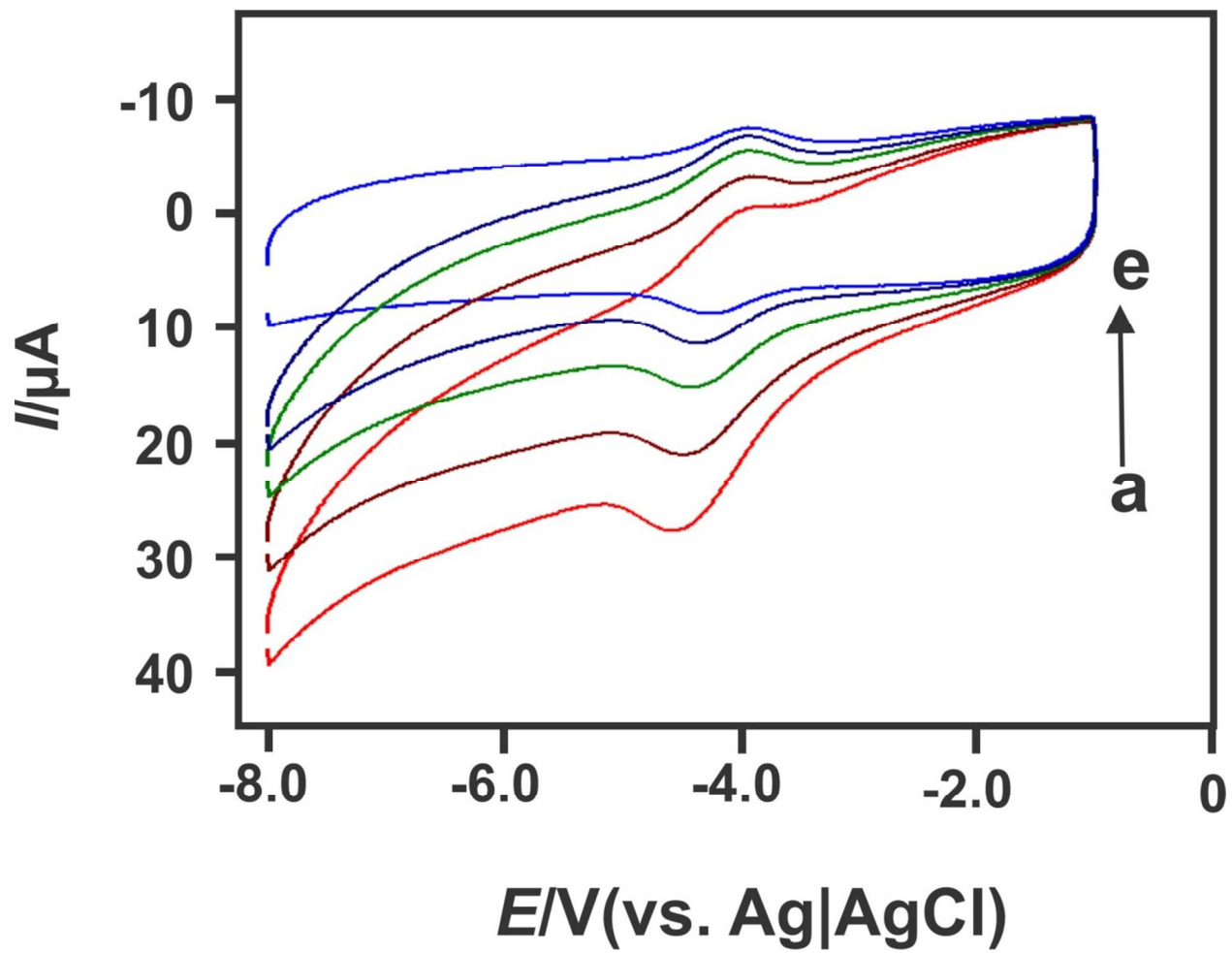


533

534

535

Fig. 4



536

537

538

Fig. 5

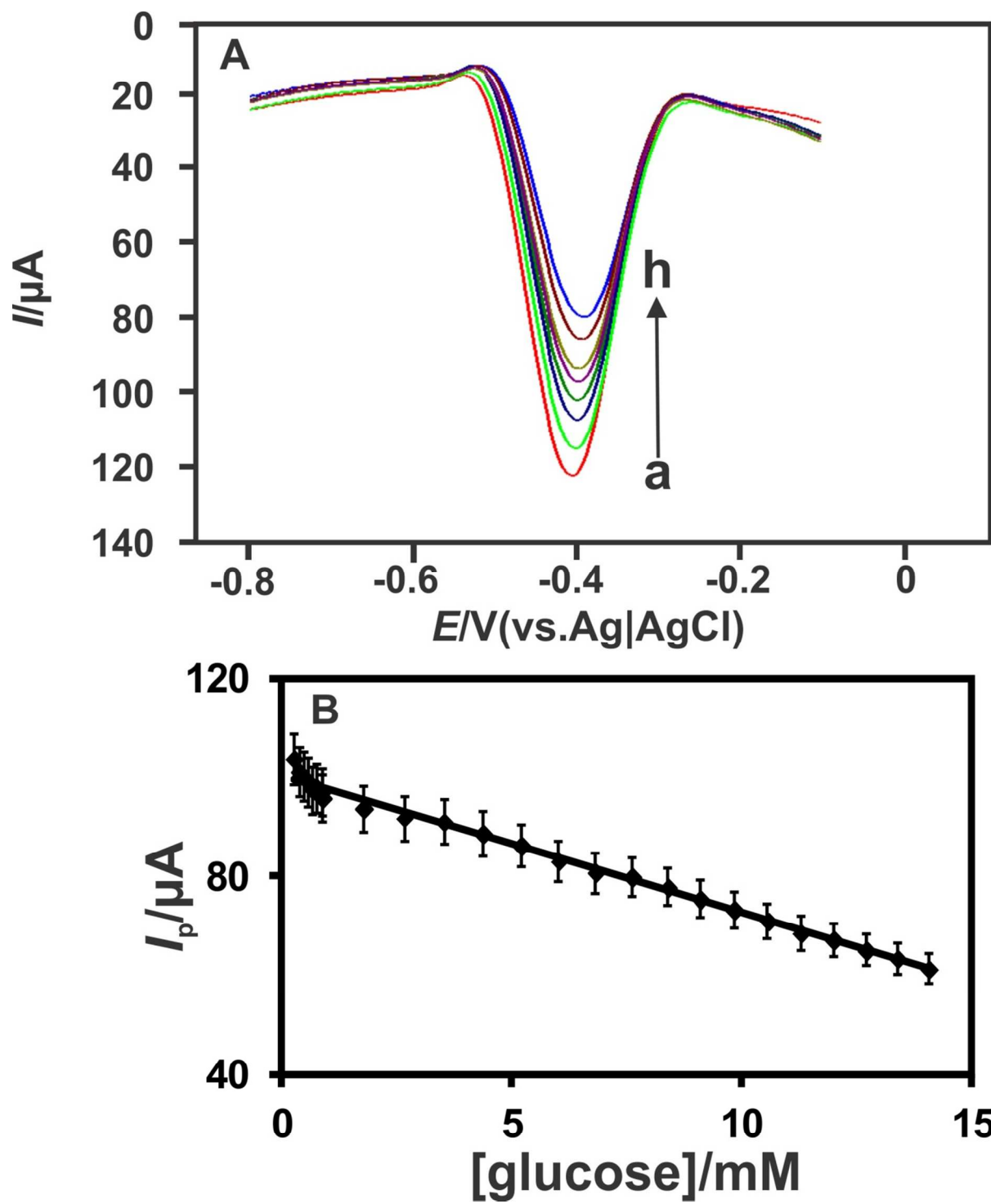


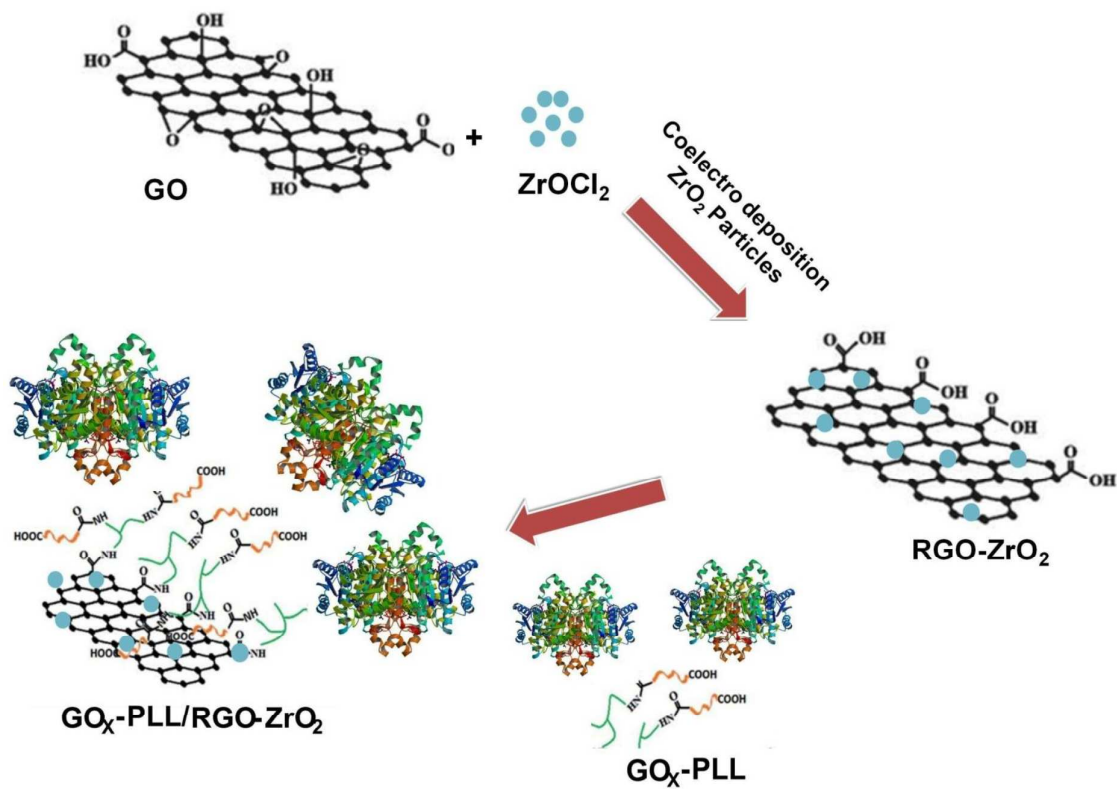
Fig. 6

539

540

541

Graphical Abstract

Schematic representation of the preparation procedure of GOx-PLL/RGO-ZrO₂ composite.